Influence of interfacial electrokinetic on MHD radiative nanofluid flow in a permeable microchannel with Brownian motion and thermophoresis effects

Article *in* Open Physics · November 2020

DOI: 10.1515/phys-2020-0161

CITATIONS
6

READS
178

7 authors, including:

Abdul Samad Khan
Northwestern Polytechnical University
7 PUBLICATIONS **83** CITATIONS

SEE PROFILE

Yufeng Nie
Northwestern Polytechnical University
188 PUBLICATIONS **1,319** CITATIONS

SEE PROFILE

Zahir Shah
University of Lakki Marwat, Khyber Pakhtunkhwa Pakistan
282 PUBLICATIONS **4,773** CITATIONS

SEE PROFILE

Research Article

Abdul Samad Khan, Yufeng Nie, Zahir Shah, Ilyas Khan*, Dumitru Baleanu, Kottakkaran Sooppy Nisar*, and Raees Khan

Influence of interfacial electrokinetic on MHD radiative nanofluid flow in a permeable microchannel with Brownian motion and thermophoresis effects

https://doi.org/10.1515/phys-2020-0161
received May 12, 2020; accepted August 22, 2020

Abstract: In this study, the behavior of a microchannel flow is examined. The fluid is considered to be a nanofluid, which moves between two parallel flat plates in the presence of an electrical double layer. The Buongiorno nanofluid is considered with body force. In this study, the unphysical supposition presented in the preceding work to the discontinuity of the flow fled where the electrostatic potential in the central of the canal must be equal to zero is removed. The incorrect supposition that the pressure constant is preserved, which is considered a known form, is corrected. The current fresh model equation is modified by using dimensionless parameters to convert partial differential equations into ordinary differential equations. The transformed nonlinear equations are solved by the homotopy analysis method. The physical parameters, magnetic parameters, Eckert number, Lewis number, Brownian motion parameters, thermophoresis parameters, and Prandtl number are analyzed. The influence of both the viscous and Joule dissipation in the presence of magnetohydrodynamic effect is examined.

Keywords: nanofluid, electrical double layer, microchannel, similarity transformation, HAM

1 Introduction

Nanofluid contains nanometer-sized particles called nanoparticles. Nanofluids are formed by the colloidal interruptions of nanoparticles in a base fluid. Nanofluids have low thermal conductivity and therefore do not attain the required freezing or heating rates. To overcome this challenge, nanoparticles are inserted in base fluids. This increases the heat transfer characteristics of nanofluids which find applications in a wide range of industrial settings such as nuclear power plants, paper production, vehicle cooling, and domestic fridges.

We know that the industrial and viscous fluids differ in their various rheological features. This type of fluid is called non-Newtonian fluid. This type of fluid has numerous applications in various fields, such as plastic manufacturing, wire coating, paper and fabric vanishing, polymer production, and food dispensation. Characterizing the behavior of such type of fluids is difficult by simply using Navier–Stokes equation. This means there is no unique relation that shows the exact behavior of the non-Newtonian fluids. Therefore, many authors propose different models of non-Newtonian fluids. In this study, we discuss the Williamson fluid model [1]. He found that this type of fluids has unique characteristics which ideal plastic and viscid fluids do not possess.

One of the primary problems of the globe is maintaining energy generation. Sunlight-based vitality gives the results the hourly sun oriented transition on the earth surface being more notable than most of the human utilization of vitality in a year. Focusing on the sunlight-based vitality has been one of the most important and interesting areas for the researchers in the past few years.

* **Corresponding author: Ilyas Khan,** Department of Mathematics, College of Science Al-Zulfi, Majmaah University, Al-Majmaah, 11952, Saudi Arabia, e-mail: i.said@mu.edu.sa
* **Corresponding author: Kottakkaran Sooppy Nisar,** Department of Mathematics, College of Arts and Sciences, Prince Sattam bin Abdulaziz University, Wadi Aldawaser, 11991, Saudi Arabia, e-mail: n.sooppy@psau.edu.sa
Abdul Samad Khan: Department of Applied Mathematics, School of Science, Northwestern Polytechnical University, Dongxiang Road, Chang'an District, Xi'an, 710129, China, e-mail: abdulsamadkhan17@mail.nwpu.edu.cn
Yufeng Nie: Department of Applied Mathematics, School of Science, Northwestern Polytechnical University, Dongxiang Road, Chang'an District, Xi'an, 710129, China, e-mail: yfnie@nwpu.edu.cn
Zahir Shah: Department of Mathematics, University of Lakki Marwat, Lakki Marwat 28420, Khyber Pakhtunkhwa, Pakistan, e-mail: zahir@ulm.edu.pk
Dumitru Baleanu: Department of Mathematics, Cankaya University, Ankara, 06790, Turkey; Institute of Space Sciences, 077125, Magurele-Bucharest, Romania; Department of Medical Research, China Medical University Hospital, China Medical University, Taichung, 40447, Taiwan, e-mail: dumitru@cankaya.edu.tr
Raees Khan: Department of Mathematics, FATA University TSD Darra Adam Khel, 26100, NMD Kohat, KP, Pakistan, e-mail: raeeskhan@fu.edu.pk

Recently, a research study suggests that adding nanoparticles to the nanofluids increases heat transmission and solar collection. Solar energy is the best source of energy due to its negligible impact on the environment [2]. One of the essential elements in our daily life is solar energy through which we get electricity, heat, and water. *Nanoparticles* are an important topic of recent research. Nanofluids are heat transmission fluids which comprise a base fluid and nanoparticles. The purpose of using nanoparticles is to increase the heat transmission of the base fluid [3]. The thermal conductivity of the base liquid increases by the Brownian motion of the nanoparticles. Magnetohydrodynamic (MHD) nanofluids have vital implications in physics, chemistry, and engineering. The MHD flow of nanofluids with radiation heat transmission and movable surface heat flux in porous media is discussed by Zhang et al. [4].

This is why the subject of heat transmission in nanofluids is of much attraction to the authors. Choi and Eastman [5] have introduced the concept of nanofluid and showed that the thermal properties of the base liquids improve significantly once nanoparticles are introduced. Despite the groundbreaking struggle, the effects of theapplication of nanoparticles to fluid flow are being explored by many scientists. Sheikholeslami et al. [6] investigated the 3D nanofluid force in the presence of a magnetic field using lattice Boltzmann method. Nithyadevi et al. [7] discussed the effect of the angle of inclination on the mixed convection of the nanofluid. Dhananjay et al. [8] studied the isothermal boundary condition of the nanoparticles in the presence of Lorentz force. Selimefendigil and Hakan [9] used the finite element method to examine the heat transfer in conjugate natural convection–condition. Hayat et al. [10] showed the impact of radioactivity on nanofluid concentrations. They showed that heat dispersion increases with an increase in thermal radioactivity. Sheikholeslami [11] studied the motion of the nanofluid in a porous semi-annulus under the influence of a magnetic field. Sheikholeslami et al. [12] investigated a two-phase nanofluid in the presence of an unsteady magnetic field. They used the homotopy perturbation method for solving the model equation. Farooq et al. [13] studied the MHD Falkner–Skan flow of the nanofluid. Shehzad et al. [14] discussed about Jeffrey nanofluid with internal heat. Abbasi et al. [15] investigated Jeffrey nanofluid under heat and mass flux conditions.

Due to various applications and consideration of microchannel flow, Kandlikar and Grande [16], Bergles et al. [17], and Thome et al. [18] introduced some alternative ways of cooling microsized devices. High applications of microchannel heat sinks using large-scale cooling microreactors for the study of organic cells and the microfluid pumps have been discussed by Safaei et al. [19] and Arani et al. [20]. Particularly, Wang and Peng [21] found that the transmission and laminar heat transformation in microchannels is strange and quite complex with a conservatively sized condition. Zhao et al. [22] discussed the heat transfer investigation of the nanofluid flow in a microchannel. Recently, some researchers studied the heat transfer flow of nanofluids for different purposes [23–33]. Anum et al. [34–36] studied mass transfer and heat transfer of Williamson and Walters-B nanofluid flow with MHD and thermal radiation. Sunil et al. [37–39] investigated the fractional Lotka–Volterra model in the Caputo sense. They converted the considered modelled equation into an algebraic equation to solve it easily. They also discussed a model to describe the velocity of the particle during Brownian motion. Khalid et al. [40] introduced an analytical and numerical study of the Peyrard–Bishop DNA dynamic model. They compared the analytical and numerical results and presented in graphs. Lu et al. [41] studied the numerical and analytical simulation of the separation phase for the ternary alloys of iron. Hadi et al. [42] used the method of exponential rational function to solve four conformable fractional Boussinesq-like equations. Osman et al. [43–47], Ahmad et al. [48], and Omar et al. [49] used the unified technique and the modified reproducing kernel discretization technique to solve different model equations. They showed that the unified method offers a powerful mathematical tool to solve the nonlinear conformable fractional evaluation equations. Jian-Guo et al. [50] studied the Hirota equation and found an exact solution. Sumit et al. [51–53] investigated the heat and mass transfer of the two-dimensional flow. The fluid they considered in their work is Williamson nanofluid with MHD. Prakash et al. [54] discussed the thermal radiation of the nanofluid flow in the presence of peristalsis electroosmosis phenomenon. The tapered asymmetric microchannels were taken into account in his work. Sharma et al. [55] investigated the MHD mixed convection flow of the non-Newtonian fluid. Gupta and Dutta [56] examined a mathematical model for HIV/AIDS and solved using the homotopy analysis method (HAM). For comparing the accuracy, they used the numerical method.

In the light of these studies, the main aim of this research is to examine the nanofluid flow of the Williamson fluid. The fluid here in this study moves between the two parallel flat plates in the presence of an electrical double layer (EDL). The Buongiorno nanofluid is considered with body force. In this study, the unphysical supposition presented in the preceding work to the discontinuity of the flow fled where the electrostatic potential in the central of the canal must be equal to zero is removed. The physical parameters have been analyzed and discussed. The influence of both the viscous and Joule dissipation in the presence of MHD effect is

examined. We choose the HAM method to solve this problem. The purpose of choosing this method is that it is a fast convergent and time-saving method and offers the choice of choosing our own auxiliary linear operator. HAM is an analytical method, which is semianalytical. We solved nonlinear ordinary differential equations by using HAM. The stated technique pays the conception of the homotopy taken from the topology, and it generates a convergent series result for nonlinear systems. This is supported by operating a homotopy Maclaurin series to compact with the nonlinearities in the system. Jagdev et al. [57,58] used a numerical scheme q-local fractional homotopy analysis transform method to solve the local fractional linear transport equation. Gupta et al. [59,60] and Das et al. [61] used HAM and a new powerful algorithm based on HAM to solve the nonlinear diffusion equation.

1.1 Analytical solution to the electrostatic potential

Viscous and Joule dissipation MHD.

The ratio between $\overset{*}{\Omega}$ and ρ_e is given below:

$$D_{yy}\overset{*}{\Omega} = -\frac{\rho_e}{\omega_o \omega}, \tag{1}$$

where ω represents the dielectric constant and ω_o represents the permittivity of the vacuum of the fluid.

Manipulating the hypothesis of the equilibrium Boltzmann dispersal around the unchanging dielectric constant and omitting the variation, the number of the ion dissemination in the symmetric electrolyte result is given by

$$n_i = n_{0i} \exp - \left(\frac{\widehat{z}_i e \overset{*}{\Omega}}{k_b \widehat{T}} \right), \tag{2}$$

where η_{0i} signify the bulk ion concentrations and $\widehat{z}_i$ signify the valence of the i type ions. The charge of a proton is denoted by e, $\overset{*}{\Omega}$ represents the electrical potential, k_b is the Boltzmann constant, and $\widehat{T}$ represents the total temperature. In a unit volume of the fluid, the average charge density is

$$\rho_e = (n_+ - n_-)\widehat{z}_i e = -2n_0 \widehat{z}_i e \sinh \left(\frac{\widehat{z}_i e \overset{*}{\Omega}}{k_b \widehat{T}} \right). \tag{3}$$

By simulating equation (3) into equation (1) (Poisson's equation), we get the famous Poisson–Boltzmann equation:

$$\frac{\mathrm{d}^2 \overset{*}{\Omega}}{\mathrm{d}y^2} = \frac{2n_0 \widehat{z}_i e}{\omega_0 \omega} \sinh \left(\frac{\widehat{z}_i e \overset{*}{\Omega}}{k_b \widehat{T}} \right). \tag{4}$$

By applying the similarity transformation, we get the nondimensionalized form of equation (4):

$$X = \frac{x}{H}, \quad Y = \frac{y}{H}, \quad \Omega(Y) = \frac{\widehat{z}_i e \overset{*}{\Omega}}{k_b \widehat{T}}, \quad \rho^* = \frac{\rho_e}{n_0 \widehat{z}_i e}, \tag{5}$$

$$\frac{\mathrm{d}^2 \Omega}{\mathrm{d}Y^2} = \kappa^2 \sinh(\Omega(Y)), \tag{6}$$

$$\frac{\mathrm{d}^2 \Omega}{\mathrm{d}Y^2} = -\frac{\kappa^2}{2} \rho^*(Y), \tag{7}$$

where $\kappa = Hk$ in which $\kappa^2 = \frac{2n_0 \widehat{z}_i^2 e^2}{(\omega_0 \omega k_b \widehat{T})}$ represents the Debye–Hückel parameter, and $1/\kappa$ represents the thickness of the EDL. A suitable boundary condition for equations (6) and (7) is given below:

$$\Omega(\pm 1) = \bar{\xi} = \frac{\widehat{z} e \xi}{k_b \widehat{T}}, \tag{8}$$

where ξ is the zeta potential which is used for the measurement of the electrical potential at the shear plane, i.e., the horizon in between diffuse film and compacted film [10].

If the electric potential is lesser than the thermal energy of the ions, i.e., $(|\widehat{z} e \overset{*}{\Omega}|) \ll |k_b \widehat{T}|$, using Debye–Hückel linear approximation, equation (6) becomes

$$\frac{\mathrm{d}^2 \Omega}{\mathrm{d}Y^2} = \kappa^2 \Omega(Y). \tag{9}$$

Analytically, it is given by

$$\Omega(Y) = \frac{\bar{\xi}}{1 + e^{2k}} [e^{\kappa(1+Y)} + e^{\kappa(1-Y)}]. \tag{10}$$

1.2 Mathematical formulation for other fields

We use horizontal rectangular microchannel with EDL and pass the nanofluid flow of heat transmission over the stated microchannel. Figure 1 shows the physical effect. X-axis is parallel to the channel of the walls, and Y-axis is perpendicular to the walls. We keep the origin fix here at the center line of the microchannel. H denotes half distance between the upper and the lower wall. Length and width of the microchannel are denoted by L and W, respectively. For simplification, consider $W \gg H$. Then, we can frame the current research problem as a nonlinear microchannel flow of two-dimension with the effect of EDL:

$$\nabla \cdot V = 0, \tag{11}$$

$$\rho(V \cdot \nabla) V = -\nabla p + \mu \nabla^2 V + F, \tag{12}$$

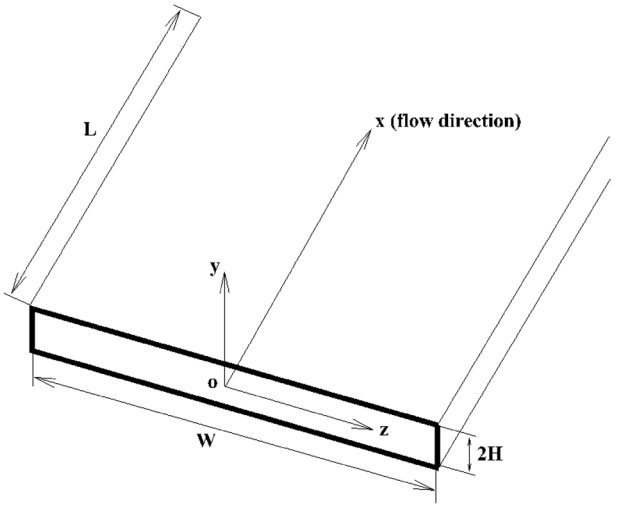

(a)

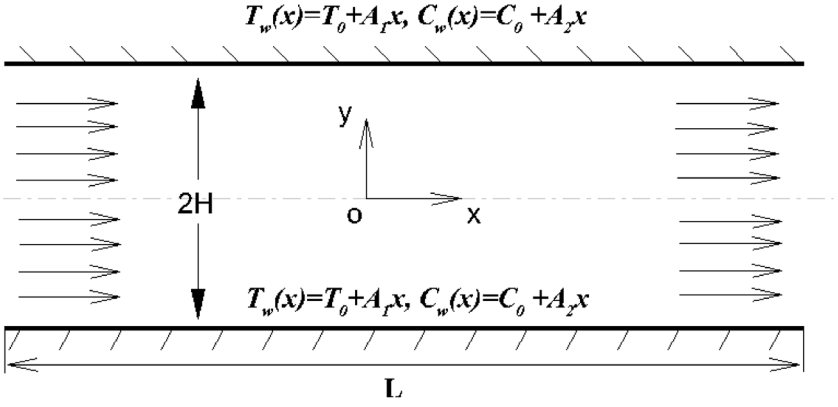

(b)

Figure 1: Geometry of the current problem: (a) geometry in 3D and (b) geometry in 2D.

$$(V\cdot\nabla)T = \alpha\nabla^2 T + \tau\left[D_B\nabla T\cdot\nabla C + \left(\frac{D_T}{T_0}\right)\nabla T\cdot\nabla T\right] + \frac{\mu}{\rho c}\Phi, \tag{13}$$

$$(V.\ \nabla)C = D_B\nabla^2 C + \left(\frac{D_T}{T_0}\right)\nabla^2 T, \tag{14}$$

where F is the electrical body force and Φ is the viscous dissipation term, which is defined as

$$\Phi = 2[(u_x)^2 + (v_y)^2 + (w_z)^2] + (v_x + u_y)^2 + (w_y + v_z)^2 + (u_z + w_x)^2 - \frac{2}{3}(u_x + v_y + w_z)^2. \tag{15}$$

If the flow is parallel in the channels, then only one component of the velocity field will not be zero. This means that the collective fluid particles move in a similar path. Only the velocity part u is nonzero; therefore, v is zero in all places. From the continuity equation, $u_x = 0$; thus, u is independent of x. In the same way, the hydraulic pressure, which is represented by p, is only dependent on the motion of the fluid, which shows that it is only a function of x, and thus the pressure gradient p_x is a constant. It is presumed that the volumetric fraction of the temperature and the nanoparticle on both walls rise or fall linearly with x, namely, $T_w(x) = T_0 + A_1x$ and $C_w(x) = C_0 + A_2x$, where T_0 represents the reference temperature and C_0 represents the volumetric fraction of the reference nanoparticle at the channel entrance. As the temperature T and volumetric fraction of the nanoparticle C vary linearly with x [21,22], we obtain $T_{xx} = C_{xx} = 0$.

With the above supposition, we see that the continuity equation is satisfied, and rest of the governing equations are simplified to the following equations:

$$\mu u_{yy} - \frac{\sigma B_0^2}{\rho}u - \frac{\nu}{k}u - p_x + E_x\rho_e = 0, \tag{16}$$

$$u_x T = \alpha T_{yy} + \tau D_B\,(T_x C_x + T_y C_y) + \frac{\tau D_T}{T_0}[(T_x)^2 + (T_y)^2] + \frac{\mu}{\rho c}(u_y)^2 - \frac{\sigma B_0^2}{\rho C_p}u^2, \tag{17}$$

$$uC_x = D_B C_{yy} + \frac{D_T}{T_0}T_{yy}, \tag{18}$$

using the boundary conditions

$$\begin{aligned} &u(\pm H) = 0, \quad T_w(\pm H) = T_0 + A_1 x,\\ &C_w(\pm H) = C_0 + A_2 x. \end{aligned} \tag{19}$$

In the channel flow study, we assumed the mass flow rate as a given number. Therefore, we get the following:

$$V_m = \frac{1}{2H}\int_{-H}^{+H} u(y)\,\mathrm{d}y = \frac{1}{H}\int_{0}^{+H} u(y)\,\mathrm{d}y, \tag{20}$$

where U_m denotes the average fluid velocity passing through the channel section. Using the dimensionless parameters,

$$V(Y) = \frac{u}{V_m}, \quad \Theta(Y) = \frac{T - T_0}{A_1 H}, \quad \Phi(Y) = \frac{C - C_0}{A_2 H}. \tag{21}$$

Nondimensionalizing equation (16) by similarity transformations (5) and (21), we get

$$\frac{\mathrm{d}^2 V}{\mathrm{d}Y^2} - K_1 - 2K_2\overline{E}_s\Omega(Y) - MV - KV = 0. \tag{22}$$

Using boundary conditions

$$V(\pm 1) = 0, \quad V\int_0^1 V(Y)\,\mathrm{d}Y = 1, \tag{23}$$

where $K_1 = \frac{H^2}{\mu V_m}P_x$, $K_2 = \frac{n_0 \widehat{e} e\xi H^2}{\mu V_m L}$, where $P_x = -\partial p/\partial x$ represents the pressure constant, $\bar{E}_s = E_s/\xi$ is the stream potential, $E_x = E_s/L$.

Substituting the nondimensional variables (21) into equations (17) and (18), we get the compact energy and concentration of nanoparticle equations as

$$\frac{\mathrm{d}^2\Theta}{\mathrm{d}Y^2} + Nb\left(1 + \frac{\mathrm{d}\Theta}{\mathrm{d}Y}\frac{\mathrm{d}\Phi}{\mathrm{d}Y}\right) + Nt\left(1 + \left(\frac{\mathrm{d}\Theta}{\mathrm{d}Y}\right)^2\right) + \mathrm{PrEc}\left(\frac{\mathrm{d}V}{\mathrm{d}Y}\right)^2 - \mathrm{Re}\,\mathrm{Pr}V - J(V)^2 = 0, \tag{24}$$

$$\frac{\mathrm{d}^2\Phi}{\mathrm{d}Y^2} + \frac{\mathrm{Nt}}{\mathrm{Nb}}\frac{\mathrm{d}^2\Theta}{\mathrm{d}Y^2} - \mathrm{RePeLe}V = 0, \tag{25}$$

subject to the boundary conditions

$$\Theta(\pm 1) = 0, \quad \Phi(\pm 1) = 0, \tag{26}$$

where $\mathrm{Nb} = \frac{\tau D_B A_2 H}{\alpha}$is the Brownian motion parameter, $\mathrm{Nt} = \frac{\tau D_T A_1 H}{\alpha T_0}$ is the thermophoresis parameter, $\mathrm{Pr} = \frac{V_m}{\alpha}$ is the Prandtl number, $\mathrm{Re} = \frac{V_m H}{\upsilon}$ is the Reynolds number, $\mathrm{Ec} = \frac{V_m^2}{cA_1 H}$ is the Eckert number, $\mathrm{Le} = \frac{\alpha}{D_B}$ is the Lewis number, $M = \frac{H^2\sigma B_0^2}{\mu\rho}$ is the magnetic parameter, $k = \frac{H^2\nu}{\mu\kappa}$ is the permeability parameter, and $J = \frac{H\sigma B_0^2}{\alpha A_1 \rho c_p}$ is a Joule dissipation term.

The main physical quantities of practical interests are the local skin friction, the local Nusselt number, and the local Sherwood number. We know that the flow inside the channel is a symmetric flow; therefore, we can consider them on the lower plate. Therefore, in the current situation, it is defined as

$$C_{f2} = \frac{\tau_{w2}}{\rho_f V_m^2}, \ \mathrm{Nu}_2 = \frac{xq_{wT2}}{k_f(T_w - T_0)}, \ \mathrm{Sh}_2 = \frac{xq_{wC2}}{D_B(C_w - C_0)}, \tag{27}$$

where

$$\begin{aligned} &\tau_{w2} = \mu u_{yy=-H}, \quad q_{wT2} = -k_f T_{yy=-H},\\ &q_{wC2} = -D_B C_{yy=-H}. \end{aligned} \tag{28}$$

Substituting equation (21) into equation (27), we get the following:

$$C_{f2} = \frac{1}{\mathrm{Re}}V'(-1), \ \mathrm{Nu}_2 = -\Theta'(-1), \ \mathrm{Sh}_2 = -\Phi'(-1). \tag{29}$$

1.3 HAM solution

We solve equations (9) and (22)–(25) using the given boundary conditions (8), (23), and (26). We use HAM in the succeeding way.

The linear operators are taken as

$$L_\Omega(\Omega) = \Omega'', \quad L_V(V) = V'', \quad L_\theta(\theta) = \theta'' \text{ and } L_\varphi(\varphi) = \varphi'', \tag{30}$$

containing the following characteristics:

$$\begin{aligned} &L_\Omega(c_1 + c_2\eta) = 0, \quad L_V(c_3 + c_4\eta) = 0,\\ &L_\theta(c_4 + c_6\eta) = 0, \quad L_\varphi(c_7 + c_8\eta) = 0, \end{aligned} \tag{31}$$

where c_i $(i = 1\text{–}8)$ are constants.

The initial assumptions are selected as follows:

$$\Omega_0(\eta) = \eta, \ V_0(\eta) = 0, \ \theta_0(\eta) = 0, \ \varphi_0(\eta) = 0. \tag{32}$$

The resulting nonlinear operators N_Ω, N_V, N_θ, N_φ are given as follows:

$$N_\Omega[\Omega(\eta;p)] = \frac{\partial^2\Omega(\eta;p)}{\partial\eta^2} - k^2\Omega(\eta;p), \tag{33}$$

$$N_V[V(\eta;p), \Omega(\eta;p)] = H^2\frac{\partial^2 V(\eta;p)}{\partial\eta^2} - K_1 - 2K_2E_s\Omega(\eta;p) - MV(\eta;p), \tag{34}$$

$$N_\theta[V(\eta;p), \theta(\eta;p), \varphi(\eta;p)] = \left(1 + \frac{4}{2}Rd\right)\frac{\partial^2\theta(\eta;p)}{\partial\eta^2} - N_b\left(1 + \frac{\partial\theta(\eta;p)}{\partial\eta}\frac{\partial\varphi(\eta;p)}{\partial\eta}\right)N_t\left(1 + \left(\frac{\partial\theta(\eta;p)}{\partial\eta}\right)^2\right) + \mathrm{PrEc}\left(\frac{\partial V(\eta;p)}{\partial\eta}\right)^2 - \mathrm{PrReV}(\eta;p) - \mathrm{PrEcM}(V(\eta;p))^2, \tag{35}$$

$$N_\varphi[V(\eta;p), \theta(\eta;p), \varphi(\eta;p)] = \frac{\partial^2\varphi(\eta;p)}{\partial\eta^2} + \frac{N_t}{N_b}\frac{\partial^2\theta(\eta;p)}{\partial\eta^2} - \mathrm{Re}\,PeLeV(\eta;p). \tag{36}$$

The detailed HAM method is discussed in ref. [1]. Here, zeroth-order problems are

$$(1-p)L_\Omega[\Omega(\eta;p) - \Omega_0(\eta)] = p\hbar_\Omega N_\Omega[\Omega(\eta;p)], \tag{37}$$

$$(1-p)L_V[V(\eta;p) - V_0(\eta)] = p\hbar_V N_V[V(\eta;p), \psi(\eta;p)], \tag{38}$$

$$(1-p)L_\theta[\theta(\eta;p) - \theta_0(\eta)] = p\hbar_\theta N_\theta[V(\eta;p), \theta(\eta;p), \varphi(\eta;p)], \tag{39}$$

$$(1-p)L_\varphi[\varphi(\eta;p) - \varphi_0(\eta)] = p\hbar_\varphi N_\varphi[V(\eta;p), \theta(\eta;p), \varphi(\eta;p)]. \tag{40}$$

The equivalent boundary conditions are

$$\begin{aligned} &\Omega(\eta;p)|_{\eta=-1} = \xi, \quad \Omega(\eta;p)|_{\eta=1} = \xi,\\ &V(\eta;p)|_{\eta=-1} = 0, \quad V(\eta;p)|_{\eta=1} = 0,\\ &\theta(\eta;p)|_{\eta=-1} = 0, \quad \theta(\eta;p)|_{\eta=1} = 0,\\ &\varphi(\eta;p)|_{\eta=-1} = 0, \quad \varphi(\eta;p)|_{\eta=1} = 0, \end{aligned} \tag{41}$$

where $p \in [0, 1]$ is the imbedding parameter, $\hbar_\Omega$,$\hbar_V$, $\hbar_\theta$, $\hbar_\varphi$ are used to control the convergence of the solution. When $p = 0$ and p = 1, we have

$$\begin{aligned} &\Omega(\eta;1) = \Omega(\eta), \quad V(\eta;1) = V(\eta),\\ &\theta(\eta;1) = \theta(\eta) \text{ and } \varphi(\eta;1) = \varphi(\eta), \end{aligned} \tag{42}$$

expanding $\Omega(\eta;p)$, $V(\eta;p)$, $\theta(\eta;p)$, $\varphi(\eta;p)$ in Taylor's series about $p = 0$:

$$\begin{aligned} \Omega(\eta;p) &= \Omega_0(\eta) + \sum_{m=1}^{\infty}\Omega_m(\eta)p^m,\\ V(\eta;p) &= V_0(\eta) + \sum_{m=1}^{\infty}V_m(\eta)p^m,\\ \theta(\eta;p) &= \theta_0(\eta) + \sum_{m=1}^{\infty}\theta_m(\eta)p^m,\\ \varphi(\eta;p) &= \varphi_0(\eta) + \sum_{m=1}^{\infty}\varphi_m(\eta)p^m, \end{aligned} \tag{43}$$

where

$$\begin{aligned} \Omega_m(\eta) &= \frac{1}{m!}\frac{\partial\Omega(\eta;p)}{\partial\eta}\bigg|_{p=0},\\ V_m(\eta) &= \frac{1}{m!}\frac{\partial V(\eta;p)}{\partial\eta}\bigg|_{p=0},\\ \theta_m(\eta) &= \frac{1}{m!}\frac{\partial\theta(\eta;p)}{\partial\eta}\bigg|_{p=0}, \quad \varphi_m(\eta) = \frac{1}{m!}\frac{\partial\varphi(\eta;p)}{\partial\eta}\bigg|_{p=0}. \end{aligned} \tag{44}$$

We choose the secondary constraints $\hbar_\Omega$, $\hbar_V$, $\hbar_\theta$, $\hbar_\varphi$ in the way that the series (43) converges at $p = 1$. Switching $p = 1$ in (43), we get the following:

$$\begin{aligned} \Omega(\eta) &= \Omega_0(\eta) + \sum_{m=1}^{\infty}\Omega_m(\eta),\\ V(\eta) &= V_0(\eta) + \sum_{m=1}^{\infty}V_m(\eta),\\ \theta(\eta) &= \theta_0(\eta) + \sum_{m=1}^{\infty}\theta_m(\eta),\\ \varphi(\eta) &= \varphi_0(\eta) + \sum_{m=1}^{\infty}\varphi_m(\eta). \end{aligned} \tag{45}$$

The mth order problem fulfills

$$\begin{aligned} L_\Omega[\Omega_m(\eta) - \chi_m\Omega_{m-1}(\eta)] &= \hbar_\Omega R_m^\Omega(\eta),\\ L_V[V_m(\eta) - \chi_m V_{m-1}(\eta)] &= \hbar_V R_m^V(\eta),\\ L_\theta[\theta_m(\eta) - \chi_m\theta_{m-1}(\eta)] &= \hbar_\theta R_m^\theta(\eta),\\ L_\varphi[\varphi_m(\eta) - \chi_m\varphi_{m-1}(\eta)] &= \hbar_\varphi R_m^\varphi(\eta). \end{aligned} \tag{46}$$

The analogous boundary conditions are as follows (Figures 2 and 3):

$$\begin{aligned} &\Omega_m(-1) = \Omega_m(1) = V_m(-1) = V_m(1) = 0,\\ &\theta_m(-1) = \theta_m(1) = \varphi_m(-1) = \varphi_m(1) = 0. \end{aligned} \tag{47}$$

Here,

$$R_m^\Omega(\eta) = \Omega_{m-1}'' - k^2\Omega_{m-1}, \tag{48}$$

$$R_m^V(\eta) = H^2V_{m-1}'' - K_1 - 2K_1E_s\Omega_{m-1} - MV_{m-1}, \tag{49}$$

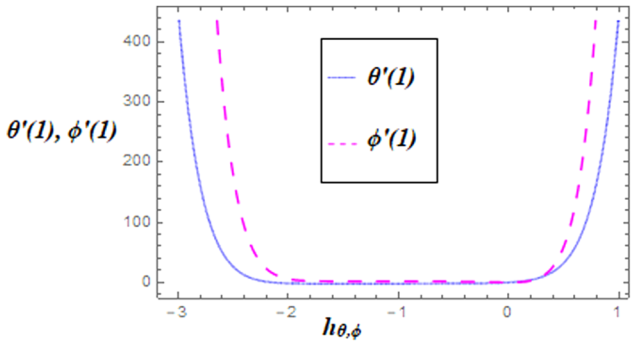

Figure 2: Combined *h*-curve graph of the temperature and concentration profiles.

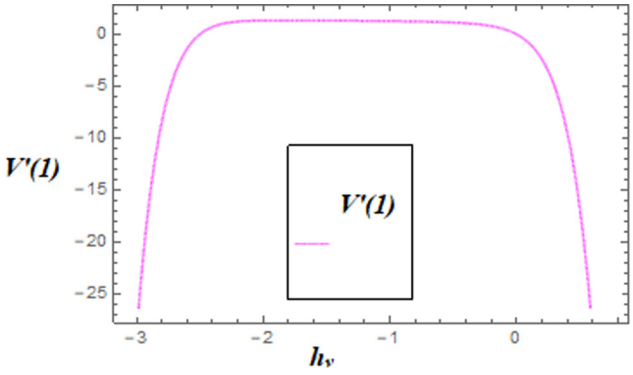

Figure 3: *h*-curve graph of the velocity profile.

$$R_m^{\theta}(\eta) = \left(1 + \frac{4}{2}Rd\right)\theta''_{m-1} + N_b\left(1 + \sum_{k=0}^{m-1}\theta'_{m-1-k}\varphi'_k\right) \times N_b\left(1 + \sum_{k=0}^{m-1}\theta'_{m-1-k}\varphi'_k\right)\mathrm{PrEc}\left(\sum_{k=0}^{m-1}V'_{m-1-k}V'_k\right) - \mathrm{PrRe}V_{m-1} - \mathrm{PrEc}M\sum_{k=0}^{m-1}V_{m-1-k}V_k, \quad (50)$$

$$R_m^{\varphi}(\eta) = \varphi'_{m-1} + \frac{N_t}{N_b}\theta''_{m-1} - \mathrm{RePeLe}V_{m-1}, \quad (51)$$

where

$$\chi_m = \begin{cases} 0, & \text{if } p \le 1 \\ 1, & \text{if } p > 1. \end{cases}$$

Figures 4 and 5 show the influence of $\kappa 1$ and $\kappa 2$ on velocity distribution $V(Y)$. An increasing behavior is noticed for both $\kappa 1$ and $\kappa 2$. The higher value of $\kappa 1$ and $\kappa 2$ augmented the velocity of nanofluid flow.

The Hartmann number is based on the Lorentz force theory. As stated by the Lorentz force theory, the larger Hartmann number means more collision among the atoms of the fluid, which produces more resistive force to fluid flow. More opposing force reduces the fluid flow, and the velocity field falls down (Figure 6).

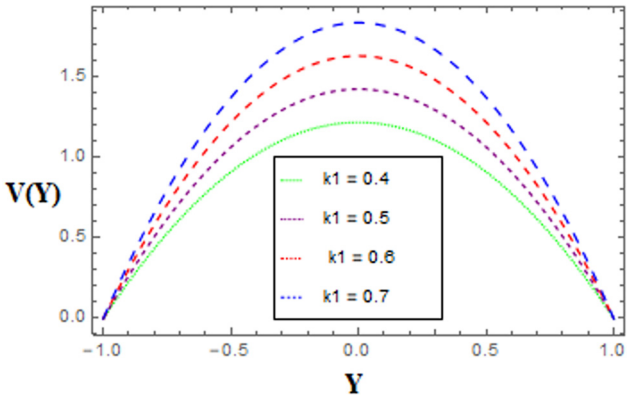

Figure 4: Variations in velocity distribution $V(Y)$ for different values of $\kappa 1$.

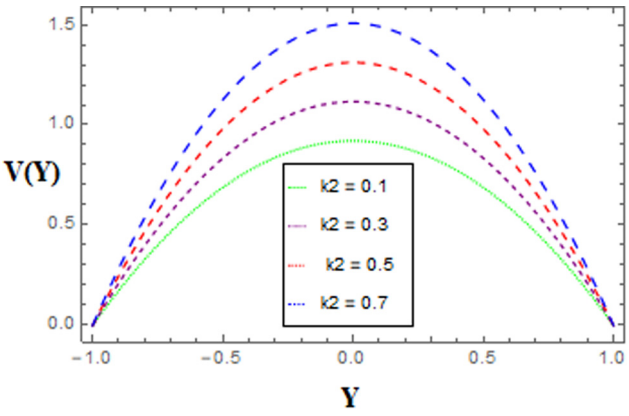

Figure 5: Variations in velocity distribution $V(Y)$ for different values of $\kappa 2$.

Figure 7 shows the Eckert number "Ec" on temperature distributions. We see that with increasing Ec, the thickness of the thermal boundary layer and temperature increase. When Ec increases, the energy of the heat is stored in the fluid, which is due to the friction forces that improve the temperature distribution.

Figure 8 shows that with increasing Lewis number, the concentration of the nanoparticle decreases, which correlates with the boundary layer thickness. It is because the Lewis number contains the coefficient of the Brownian dispersion. The coefficient of the Brownian dispersion is stronger for smaller values of the Lewis number and weaker for greater values of the Lewis number. Such type of weaker Brownian dispersion coefficient leads to a lower nanoparticle concentration distribution function.

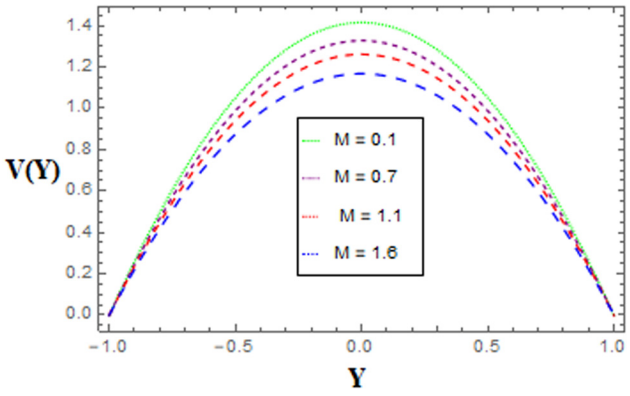

Figure 6: Variations in velocity distribution $V(Y)$ for different values of M.

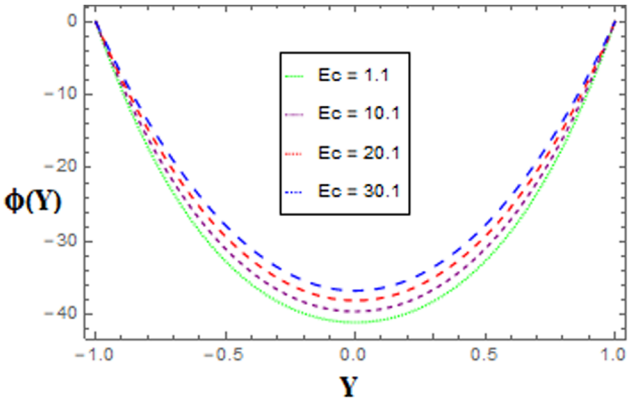

Figure 7: Variations in concentration distribution $\phi(Y)$ for different values of Ec.

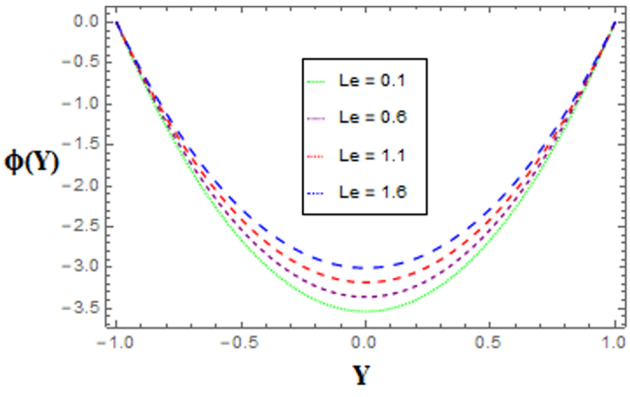

Figure 8: Variations in concentration distribution $\phi(Y)$ for different values of Le.

Figure 9 shows that higher Brownian motion causes arbitrary motion of the particles. Due to this arbitrary motion, extra heat is created. Thus, the reduction in concentration filed is depicted.

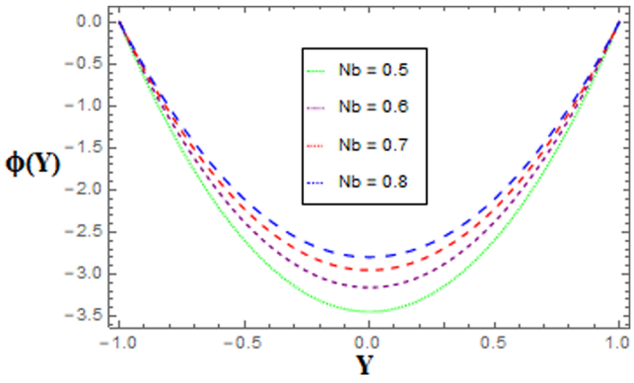

Figure 9: Differences in the concentration distribution $\phi(Y)$ for different values of Nb.

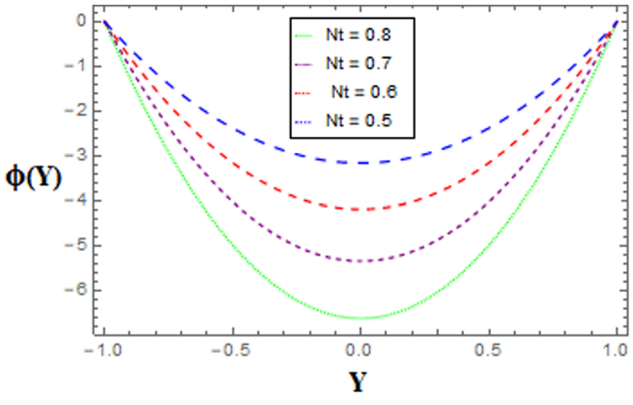

Figure 10: Variations in concentration distribution $\phi(Y)$ for different values of Nt.

Figure 10 shows that increasing Nt increases the concentration field, whereas in thermophoresis phenomena, small particles of the fluid are dragged from the hot to the cold surface. Thus, the particles of the fluid moved back from the surface, which is heated, and consequently, $\phi(Y)$ increases.

The correlation governing kinetic energy of the flow and enthalpy difference is called the Eckert number. Eckert number is used in extraordinary speed compressible flow. The positive Eckert number indicates cooling of the wall, and consequently, the heat transmission convection to the fluid is intensified.

The higher Brownian motion causes arbitrary motion of the particles. Due to this arbitrary motion, extra heat is created. Thus, escalation in temperature filed is depicted.

In thermophoresis phenomena, the small particles of the fluid are dragged from the hot to the cold surface. Thus, the particles of the fluid moved back from the surface, which is heated, and consequently, $\theta(Y)$ increases.

Table 1: Numerical values of the skin friction for various parameters

H	Es	M	$C_{f2} = \frac{1}{Re}V'(-1)$
0.5	0.6	0.6	−0.407027
0.6	0.6	0.6	−0.400427
0.7	0.6	0.6	−0.392627
0.5	0.6	0.6	−0.407027
0.5	0.7	0.6	−0.382364
0.5	0.8	0.6	−0.357702
0.5	0.6	0.6	−0.407027
0.5	0.6	0.7	−0.400893
0.5	0.6	0.8	−0.403960

Table 2: Numerical values of Nusselt number for different parameters

Rd	Nb	Nt	Pr	$-\Theta'(-1)$
0.5	0.6	0.6	0.7	−1.31073
0.6	0.6	0.6	0.7	−1.27073
0.7	0.6	0.6	0.7	−1.23073
0.5	0.6	0.6	0.7	−1.31073
0.5	0.7	0.6	0.7	−1.52740
0.5	0.8	0.6	0.7	−1.41907
0.5	0.6	0.6	0.7	−1.31073
0.5	0.6	0.7	0.7	−1.52740
0.5	0.6	0.8	0.7	−1.41907
0.5	0.6	0.6	0.7	−1.31073
0.5	0.6	0.6	0.8	−1.31380
0.5	0.6	0.6	0.9	−1.31227

Table 3: Numerical values of Sherwood number for different parameters

Pe	Nb	Nt	Re	$-\phi'(-1)$
0.5	0.6	0.6	0.5	0.293560
0.6	0.6	0.6	0.5	0.294480
0.7	0.6	0.6	0.5	0.295400
0.5	0.6	0.6	0.5	0.293560
0.5	0.7	0.6	0.5	0.273971
0.5	0.8	0.6	0.5	0.277900
0.5	0.6	0.6	0.5	0.293560
0.5	0.6	0.7	0.5	0.374567
0.5	0.6	0.8	0.5	0.462067
0.5	0.6	0.6	0.5	0.293560
0.5	0.6	0.6	0.6	0.293560
0.5	0.6	0.6	0.7	0.294480

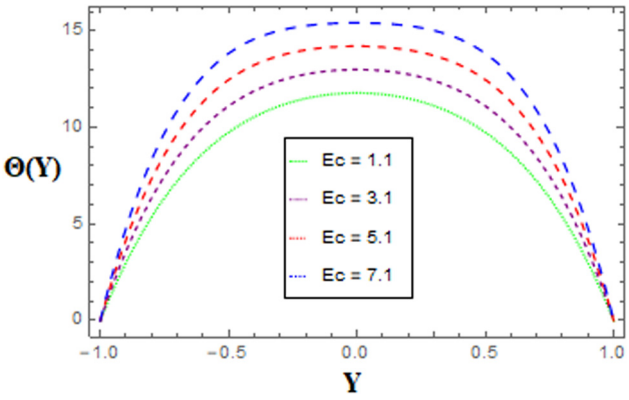

Figure 11: Variations in temperature distribution $\theta(Y)$ for different values of Ec.

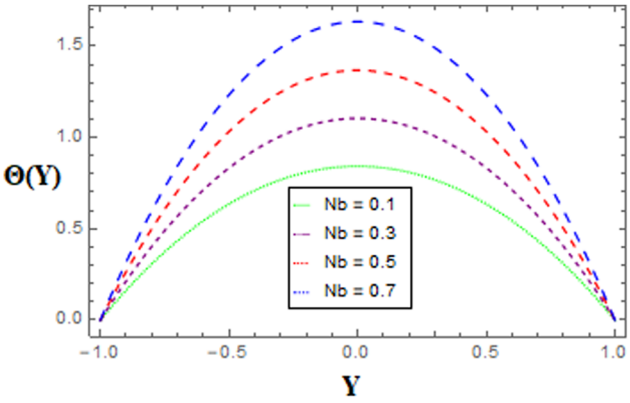

Figure 12: Disparities in temperature distribution $\theta(Y)$ for different values of Nb.

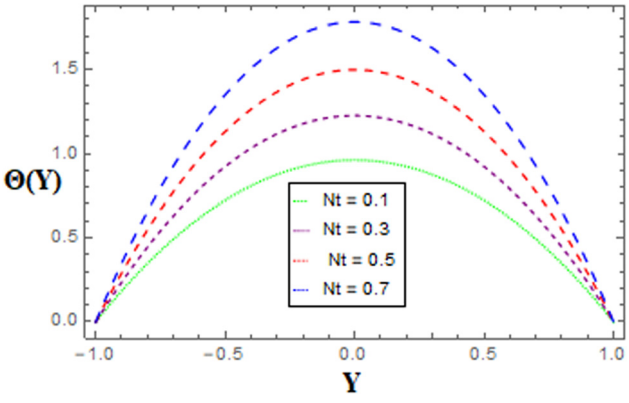

Figure 13: Variations in temperature distribution $\theta(Y)$ for different values of Nt.

The Pr has opposite impacts on the temperature of the fluid flow. The higher Pr reduces while the lower Pr increases the fluid temperature. Thus, the fluid temperature reduces with small Prandtl numbers.

The numerical calculations of surface drag force at different values of Es and M are presented in Table 1. We see that the surface drag force is reduced when Es and M increase. The numerical calculation of the heat flux at

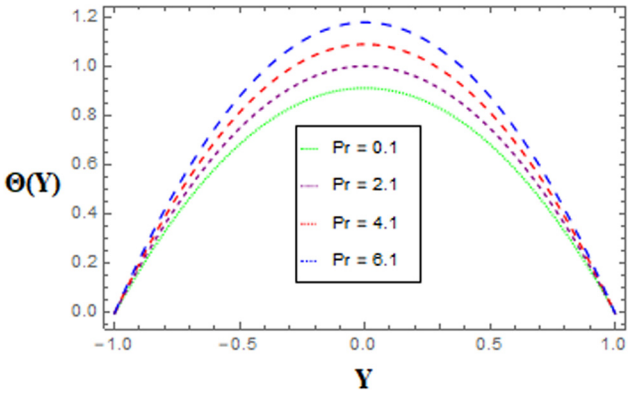

Figure 14: Deviations in temperature profile $\theta(Y)$ for different values of Pr.

different values of Nb, Nt, and Pr is presented in Table 2. With increasing Nb, Nt, and Pr, the heat flux increases. From Table 3, we observe that Sherwood number increases with increasing Nb, Nt, and Re (Figures 11–14).

2 Conclusions

In this article, the behavior of the microchannel nanofluid flow between the two parallel flat plates in the presence of EDL was examined. The Buongiorno nanofluid with body force was assumed. The model equations were solved analytically through HAM. Important model parameters were discussed graphically and numerically. Conclusions are as follows:

- The larger Hartmann number means more collision among the atoms of the fluid, which produces a more resistive force to fluid flow. The more opposing force reduces the fluid flow, and the velocity field falls down.
- Thermal dispersion reduces the heat transmission rate while the salutal dispersion is responsible for the decrease in the mass transmission rate.
- The higher Pr decreases while the lower Pr increases the fluid temperature.
- Temperature field increases the magnitude of Nt as well as the thermophoresis Nb parameters.
- Sharp drop is seen in the nanoparticle concentration profile with an increase in Nt although a small increase is seen with an increase in the value of Nb.
- The result of the viscid indulgence effect on the fluid temperature distribution and the nanoparticle concentration is important. It is because the strength of the shear and the resistance of the friction are significantly increased in the microchannel. It makes the viscous dissipation function strong.

Acknowledgments: The authors extend their thanks to the Deanship of Scientific Research at Majmaah University for funding this work under Project No. (RGP-2019-3).

Conflict of interest: None.

References

[1] Williamson RV. The flow of pseudoplastic materials. Int J Ind Eng Chem. 1929;21:1108–11.
[2] Sharma A, Tyagi VV, Chen CR, Buddhi D. Review on thermal energy storage with phase change materials and applications. Renewable Sustainable Energy Rev. 2009;13:318–45.
[3] Choi SUS. Enhancing thermal conductivity of fluids with nanoparticles. ASME Int Mech Eng. 1995;66:99–105.
[4] Zhang C, Zheng L, Zhang X, Chen G. MHD flow and radiation heat transfer of nanofluids in porous media with variable surface heat flux and chemical reaction. Appl Math Comput. 2015;39:165–81.
[5] Choi SUS, Eastman JA. Enhancing thermal conductivity of fluids with nanoparticles. Conf ASME Publ. 1995;231: 99–106.
[6] Sheikholeslami M, Hayat T, Alsaedi A. Numerical simulation of nanofluid forced convection heat transfer improvement in existence of magnetic field using lattice Boltzmann method. Int J Heat Mass Transf. 2017;108:1870–83.
[7] Nithyadevi N, Shamadhani BA, Hakan FO, Khaled AS. Effects of inclination angle and non-uniform heating on mixed convection of a nanofluid filled porous enclosure with active mid-horizontal moving. Int J Heat Mass Transf. 2017;104:1217–28.
[8] Dhananjay Y, Junye W, Rama B, Jinho L, Hyung HC. Numerical investigation of the effect of magnetic field on the onset of nanofluid convection. Appl Therm Eng. 2016;103:1441–9.
[9] Selimefendigil F, Hakan FÖ. Conjugate natural convection in a cavity with a conductive partition and filled with different nanofluids on different sides of the partition. J Mol Liq. 2016;216:67–77.
[10] Hayat T, Waqas M, Shehzad SA, Alsaedi A. A model of solar radiation and Joule heating in magnetohydrodynamic (MHD) convective flow of thixotropic Nanofluid. J Mol Liq. 2016;215:704–10.
[11] Sheikholeslami M. Influence of Lorentz forces on nanofluid flow in a porous cylinder considering Darcy model. J Mol Liq. 2017;225:903–12. doi: 10.1016/j.molliq.2016.11.022.
[12] Sheikholeslami M, Hatami M, Domairry G. Numerical simulation of two phase unsteady nanofluid flow and heat transfer between parallel plates in presence of time dependent magnetic field. J Taiwan Inst Chem Eng. 2015;46:43–50. doi: 10.1016/j.jtice.2014.09.025.
[13] Farooq U, Zhao YL, Hayat T, Alsaedi A, Liao SJ. Application of the HAM-based Mathematica package BVPh 2.0 on MHD Falkner-Skan flow of Nanofluid. Comput Fluids. 2015;11:69–75.
[14] Shehzad SA, Abdullah Z, Alsaedi A, Abbasi FM, Hayat T. Thermally radiative three-dimensional flow of Jeffrey nanofluid with internal heat generation and magnetic field. J Magn Magn Mater. 2016;397:108–14.

[15] Abbasi FM, Shehzad SA, Hayat T, Alsaedi A, Mustafa AO. Influence of heat and mass flux conditions in hydromagnetic flow of Jeffrey Nanofluid. AIP Adv. 2015;5:037111.
[16] Kandlikar SG, Grande WJ. Evolution of microchannel flow passages thermohydraulic performance and fabrication technology. Heat Transf Eng. 2002;25(1):3–17.
[17] Bergles AE, Lienhard JH, Kendall GE, Griffith P. Boiling and evaporation in small diameter channels. Heat Transf Eng. 2003;24(1):18–40.
[18] Thome JR, Dupont V, Jacobi AM. Heat transfer model for evaporation in microchannels. Part I: presentation of the model. Int J Heat Mass Transf. 2004;47(14–16):3375–85.
[19] Safaei MR, Gooarzi M, Akbari OA, Shadloo MS, Dahari M. Performance evaluation of nanofluids in an inclined ribbed microchannel for electronic cooling applications. Electron Cooling. 2016. doi: 10.5772/62898.
[20] Arani AAA, Akbari OA, Safaei MR, Marzban A, Alrashed AAAA. Heat transfer improvement of water/single-wall carbon nanotubes (SWCNT) nanofluid in a novel design of a truncated double-layered microchannel heat sink. Int J Heat Mass Transf. 2017;113:780–95.
[21] Wang BX, Peng XF. Experimental investigation on liquid forced-convection heat transfer through microchannels. Int J Heat Mass Transf. 1994;37:73–82.
[22] Zhao Q, Xu H, Tao L. Nanofluid flow and heat transfer in a microchannel with interfacial electrokinetic effects. Int J heat mass Transf. 2018;124:158–67.
[23] Jiang-Tao H, Xiu-Hong R, Di L, Fu-Yun Z, Han-Qing W. Natural convective heat and moisture transfer in an inclined building enclosure with one slender wall of finite thickness: analytical investigation and non-unique steady flow solutions. Int J Heat Mass Transf. 2017;104:1160–76.
[24] Sheikholeslami M. Magnetic source impact on nanofluid heat transfer using CVFEM. Neural Comput Appl. 2016;30(4):1055–64. doi: 10.1007/s00521-016-2740-7.
[25] Sheikholeslami M. CVFEM for magnetic nanofluid convective heat transfer in a porous curved enclosure. Eur Phys J Plus. 2016;131:413. doi: 10.1140/epjp/i2016-16413-y.
[26] Sheikholeslami M, Houman BR. Nanofluid two phase model analysis in existence of induced magnetic field. Int J Heat Mass Transf. 2017;107:288–99.
[27] Sheremet MA, Pop I, Bachok N. Effect of thermal dispersion on transient natural convection in a wavy-walled porous cavity filled with a nanofluid: Tiwari and Das' nanofluid model. Int J Heat Mass Transf. 2016;92:1053–60.
[28] Sheikholeslami M, Hayat T, Alsaedi A, Abelman S. EHD nanofluid force convective heat transfer considering electric field dependent viscosity. Int J Heat Mass Transf. 2017;108:2558–65. doi: 10.1016/j.ijheatmasstransfer.2016.10.099.
[29] Sheikholeslami M, Hayat T, Alsaedi A. Numerical study for external magnetic source influence on water based nanofluid convective heat transfer. Int J Heat Mass Transf. 2016;106:745–55. doi: 10.1016/j.ijheatmasstransfer.2016.09.077.
[30] Jashim Uddin Md, Kabir OMN, Anwar B. Computational investigation of Stefan blowing and multiple-slip effects on buoyancy-driven bioconvection nanofluid flow with microorganisms. Int J Heat Mass Transf. 2016;95:116–30.
[31] Sheikholeslami M, Rashidi MM, Hayat T, Ganji DD. Free convection of magnetic nanofluid considering MFD viscosity effect. J Mol Liq. 2016;218:393–9.
[32] Sheikholeslami M, Ganji DD. Nanofluid convective heat transfer using semi analytical and numerical approaches. A review. J Taiwan Inst Chem Eng. 2016;65:43–77.
[33] Sheikholeslami M, Chamkha, Ali J. Flow and convective heat transfer of a ferro-nanofluid in a double-sided lid-driven cavity with a wavy wall in the presence of a variable magnetic field. Numer Heat Transfer Part A. 2016;69(10):1186–200. doi: 10.1080/10407782.2015.1125709.
[34] Anum S, Hammouch Z, Sindhu TN. Bioconvective MHD flow of tangent hyperbolic nanofluid with newtonian heating. Int J Mech Sci. 2017;133:759–66.
[35] Anum S, Rashidi MM, Hammouch Z, Ilyas K. Analytical investigation of stagnation point flow of Williamson liquid with melting phenomenon. Phys Scr. 2019;94(3):035204.
[36] Anum S, Hammouch Z, Ali T. Impact of radiation in a stagnation point flow of Walters' B fluid towards a Riga plate. Therm Sci Eng Prog. 2018;6:27–33.
[37] Sunil K, Ranbir K, Ravi PA, Bessem S. A study of fractional Lotka–Volterra population model using Haar wavelet and Adams–Bashforth–Moulton methods. Math Meth Appl Sci. 2020;43(8):5564–78.
[38] Sunil K, Surath G, Mansour SML, Bessem S. A model for describing the velocity of a particle n Brownian motion y Robotnov function based fractional operator. Alex Eng J. 2020;59(3):1435–49.
[39] Sunil K, Ali A, Ranbir K, Devendra K, Jagdev S, Dumitru B, et al. An efficient numerical method for fractional SIR epidemic model of infectious disease by using Bernstein wavelets. Mathematics. 2020;8(4):558.
[40] Khalid KA, Carlo C, Gomez-Aguilar JF, Dumitru B, Osman MS. Analytical and numerical study of the DNA dynamics arising in oscillator-chain of Peyrard-Bishop model. Chaos Solitons Fractals. 2020;139:110089.
[41] Lu D, Osman MS, Khater MMA, Attia RAM, Baleanu D. Analytical and numerical simulations for the kinetics of phase separation in iron (Fe–Cr–X (X = Mo, Cu)) based on ternary alloys. Phys A Stat Mech Appl. 2020;537:122634.
[42] Hadi R, Osman MS, Mostafa E, Mohammad M, Qin Z, Seyed AB, et al. Hyperbolic rational solutions to a variety of conformable fractional Boussinesq–Kuje equations. Nonlinear Eng. 2018;8(1):224–30.
[43] Osman MS, Hadi R, Mostafa E. Traveling wave solutions for (3 + 1) dimensional conformable fractional Zakharov–Kuznetsov. Nonlinear Eng. 2019;8(1):559–67.
[44] Osman MS. New analytical study of water waves described by coupled fractional variant Boussinesq equation in fluid dynamics. Pramana – J Phys. 2019;93(2):26.
[45] Osman MS, Dianchen L, Mostafa MAK. A study of optical wave propagation in the nonautonomous Schrodinger–Hirota equation with power-Law nonlinearity. Results Phys. 2019;13:102157.
[46] Osman MS, Abdul-Majid W. A general bilinear form to generate different wave structures of solitons for a (3 + 1)-dimensional Boiti–Leon–Manna–Pempinelli equation. Math Meth Appl Sci. 2019;42(18):6277–83.

[47] Osman MS, Lu D, Khater MMA, Attia RAM. Complex wave structures for abundant solutions related to the complex Ginzburg–Landau model. Opt Int J Light Electron Opt. 2019;192:162927.
[48] Ahmad J, Nauman R, Osman MS. Multi-solitons of thermophoretic motion equation depicting the wrinkle propagation in substrate-supported graphene sheets. Commun Theor Phys. 2019;71(4):362–6.
[49] Omar AA, Osman MS, Abdel-Haleem AA, Abdel-Baset AM, Shaher M. A numerical algorithm for the solutions of ABC singular Lane–Emden type models arising in astrophysics using reproducing Kernel Discretization method. Mathematics. 2020;8(6):923.
[50] Jian-Guo L, Osman MS, Wen-Hui Z, Li Z, Guo-Ping A. Different complex wave structures described by the Hirota equation with variable coefficients in inhomogeneous optical fibers. Appl Phys B. 2019;125(9):175.
[51] Sumit G, Devendra K, Jagdev S. Analytical study for MHD flow of Williamson nanofluid with the effects of variable thickness, nonlinear thermal radiation and improved Fourier's and Fick's Laws. SN Appl Sci. 2020;2:438.
[52] Sumit G, Devendra K, Jagdev S. Magnetohydrodynamic three dimensional boundary layer flow and heat transfer of Water driven Copper and Alumina nanoparticles induced by convective conditions. Int J Mod Phys B. 2019;33(26):1950307.
[53] Sumit G, Devendra K, Jagdev S. MHD mixed convective stagnation point flow and heat transfer of an incompressible nanofluid over an inclined stretching sheet with chemical reaction and radiation. Int J Heat Mass Transf. 2018;118:378–87.
[54] Prakash J, Sharma A, Tripathi D. Thermal radiation effects on electroosmosis modulated peristaltic transport of ionic nanoliquids in biomicrofluidics channel. J Mol Liq. 2018;249:843–55.
[55] Sharma B, Kumar S, Paswan MK. Analytical solution for mixed convection and MHD flow of electrically conducting non-Newtonian nanofluid with different nanoparticles: A comparative study. Int J Heat Technol. 2018;36(3):987–96.
[56] Gupta PK, Dutta A. A mathematical model on HIV/AIDS with fusion effect: Analysis and homotopy solution. Eur Phys J Plus. 2019;134(6):265.
[57] Jagdev S, Devendra K, Sunil K. An efficient computational method for local fractional transport equation occurring in fractal porous media. Comput Appl Math. 2020;39:137.
[58] Jagdev S, Devendra K, Ram S, Sunil K. An efficient computational approach for time-fractional Rosenau–Hyman equation. Neural Comput Appl. 2018;30(10):3063–70.
[59] Gupta PK, Verma S. A numerical study of the nonlinear reaction–diffusion equation with different type of absorbent term by Homotopy analysis method. Z Naturforschung A-Journal Phys Sci. 2012;67A:621–7.
[60] Gupta KP. An approximate analytical solution of nonlinear fractional diffusion equation by homotopy analysis method. Int J Phys Sci. 2011;6(34):7721–8.
[61] Das S, Vishal K, Gupta PK, Yildirim A. An approximate analytical solution of time-fractional telegraph equation. Appl Math Comput. 2011;217(18):7405–11.